

# Quantum characterization of superconducting photon counters

**Giorgio Brida, Luigi Ciavarella, Ivo Pietro Degiovanni, Marco Genovese, Lapo Lolli, Maria Griselda Mingolla ‡, Fabrizio Piacentini, Mauro Rajteri, Emanuele Taralli**

INRIM, Strada delle Cacce 91, Torino I-10135, Italy

**Matteo G. A. Paris**

Dipartimento di Fisica, Università degli Studi di Milano, I-20133 Milano, Italy and  
CNISM, Udr Milano, I-20133 Milan, Italy

**Abstract.** We address the quantum characterization of photon counters based on transition-edge sensors (TESs) and present the first experimental tomography of the positive operator-valued measure (POVM) of a TES. We provide the reliable tomographic reconstruction of the POVM elements up to 11 detected photons and  $M = 100$  incoming photons, demonstrating that it is a linear detector.

PACS numbers: 42.50.Dv, 42.50.Ar, 03.65.Ta, 85.60.Gz

‡ also at Dipartimento di Fisica, Politecnico di Torino, Corso Duca degli Abruzzi 24, Torino I-10129, Italy

## 1. Introduction

The possibility of discriminating the number of impinging photons on a detector is a fundamental tool in many different fields of optical science and technology [1], including nanopositioning and the redefinition of candela unit in quantum metrology [2, 3], foundations of quantum mechanics [4], quantum imaging [5] and quantum information [6, 7, 8, 9], e.g for communication and cryptography. As a matter of fact, conventional single-photon detectors can only distinguish between zero and one (or more) detected photons, with photon number resolution that can be obtained by spatially [10] or temporally [11] multiplexing this kind of on/off detectors.

Genuine Photon Number Resolving (PNR) detectors needs a process intrinsically able to produce a pulse proportional to the number of absorbed photons. In fact, detectors with PNR capability are few, e.g. photo-multiplier tubes [12], hybrid photo-detectors [13] and quantum-dot field-effect transistors [14]. At the moment, the most promising genuine PNR detectors are the visible light photon counters [15] and Transition Edge Sensors (TESs) [16, 17, 18, 19, 20, 21], i.e. microcalorimeters based on a superconducting thin film working as a very sensitive thermometer [22].

For a practical application of these detectors it is crucial to achieve their precise characterization [23, 24, 25, 26, 27, 28, 29, 30]. In particular, it is generally assumed that TESs are linear photon counters, with a detection process corresponding to a binomial convolution. It is also expected that dark counts are not present in TESs. Taken together, these assumptions allow one to characterize a TES by a single number assessing the quantum efficiency of the detector, i.e. the probability  $0 \leq \eta \leq 1$  that a photon impinging onto the detector is actually revealed. In this paper, we present the first experimental reconstruction of the POVM describing the operation of a TES and, in turn, the first demonstration of the linearity. In section 2 we illustrate the method used for POVM reconstruction, while in section 3 we describe the experimental implementation. In section 4 we discuss the results and close the paper with some concluding remarks.

## 2. POVM reconstruction technique

As TESs are microcalorimeters, they are intrinsically phase insensitive detectors. In the following we thus assume that the elements of the positive operator-value measurement (POVM)  $\{\Pi_n\}$  are diagonal operators in the Fock basis, i.e.

$$\Pi_n = \sum_m \Pi_{nm} |m\rangle\langle m|, \quad (1)$$

with completeness relation  $\sum_n \Pi_n = \mathbf{I}$ . Matrix elements  $\Pi_{nm} = \langle m|\Pi_n|m\rangle$  describe the detector response to  $m$  incoming photons, i.e. the probability of detecting  $n$  photons with  $m$  photons at the input<sup>§</sup>. A reconstruction scheme for  $\Pi_{nm}$ , i.e. a tomography of

<sup>§</sup> This corresponds to consider our TES as a *grey box* (instead of a black box), on the basis of this solid physics assumption, i.e. the fact that they are microbolometers. On the other hand, trying to

the POVM, provides the characterization of the detector at the quantum level. In order to achieve the tomography of the TES POVM, we exploit an effective and statistically reliable technique [31, 32, 33] based on recording the detector response for a known and suitably chosen set of input states, e.g. an ensemble of coherent signals providing a sample of the Husimi Q-function of the elements of the POVM.

Let us consider a set of  $K$  coherent states of different amplitudes  $|\alpha_j\rangle$ ,  $j = 1, \dots, K$ . The probability of obtaining the outcome  $n$  from the TES, i.e. of detecting  $n$  photons, with the  $j$ -th state as input is given by

$$p_{nj} = \text{Tr}[|\alpha_j\rangle\langle\alpha_j|\Pi_n] = \sum_m \Pi_{nm} q_{mj} \quad (2)$$

where  $q_{mj} = \exp(-\mu_j)\mu_j^m/m!$  is the ideal photon statistics of the coherent state  $|\alpha_j\rangle$ ,  $\mu_j = |\alpha_j|^2$  being the average number of photons. In order to reconstruct the matrix elements  $\Pi_{nm}$ , we sample the probabilities  $p_{nj}$  and invert the statistical model composed by the set of Eqs. (2). Since the Fock space is infinite dimensional, this estimation problem contains, in principle, an infinite number of unknowns.

A suitable truncation at a certain dimension  $M$  should be performed, with the constraint that the probability of having  $m \geq M$  photons in the states  $|\alpha_j\rangle$  is not too large. In other words, given the set of probing coherent states, we have a little amount of data for the entries with  $m \geq M$  and we cannot investigate the performances of the detector above the corresponding energy regimes.

The distributions  $p_{nj}$  in Eq. (2) provide a sample of the Q-functions  $\langle\alpha_j|\Pi_n|\alpha_j\rangle$  of the POVM elements, and any reconstruction scheme for the  $\Pi_{nm}$  basically amounts to recover the Fock representation of the  $\Pi_n$ 's from their phase space Q-representation. In general, this cannot be done exactly due to singularity of the antinormal ordering of Fock number projectors  $|n\rangle\langle n|$  [34]. On the other hand, upon exploiting the truncation described above, we deal with POVM elements expressed as finite mixture of Fock states, which are amenable to reconstruction [35, 36]. The statistical model in (2) may be solved using maximum likelihood (ML) methods or a suitable approximation of ML. We found that reliable results are obtained already with a least squares fit, i.e we have effectively estimated  $\Pi_{nm}$  by minimization of a regularized version of the square difference  $\sum_{nj} (\sum_{m=0}^{M-1} q_{mj} \Pi_{nm} - p_{nj})^2$  where the physical constraints of smoothness is implemented by exploiting a convex, quadratic and device-independent function [32]. We also force normalization  $\sum_{n=0}^{11} \Pi_{nm} = 1$ ,  $\forall m$ , where the last POVM element is defined as  $\Pi_{11} = 1 - \sum_{n=0}^{10} \Pi_n$ .

### 3. Experiment

The TES we have characterized is composed by a  $\sim 90$  nm thick Ti/Au film [37, 38], fabricated by e-beam deposition on silicon nitride substrates. The effective sensitive area, obtained by lithography and chemical etching, is  $20 \times 20 \mu\text{m}$ . The superconducting find an experimental evidence of this phase-insensitiveness assumption is pointless, as there is not a phase reference (e.g. from the TES itself) to modify the phase of our probe states with respect to it.

wirings of Al, with thicknesses between 100 nm and 150 nm, have been defined by a lift-off technique combined with RF sputtering of the superconducting films. Upon varying the top Ti film thickness, the critical temperatures of these TESs can range between 90 mK and 130 mK, showing a sharp transition (1-2 mK).

The characterization of TES has been carried out in a dilution refrigerator with a base temperature of 30 mK. Furthermore, the detector is voltage biased, in order to take advantage of the negative Electro-Thermal Feedback, providing the possibility to obtain a self-regulation of the bias point without a fine temperature control and reducing the detector response time. The read-out operations on our TES is performed with a DC-SQUID current sensor [39]. Using room temperature SQUID electronics, we bias our device and read out the current response. Finally, the SQUID output is addressed to a LeCroy 400 MHz oscilloscope, performing the data acquisition, first elaboration and storage. In our experiment, we have illuminated the TES with a power-stabilized fiber coupled pulsed laser at  $\lambda = 1570$  nm (with a pulse duration of 37 ns and a repetition rate of 9 kHz), whose pulse is also used to trigger the data acquisition for a temporal window of 100 ns. The laser pulse energy ( $365 \pm 2$ ) pJ is measured by a calibrated power meter, and then attenuated to photon counting regime exploiting two fiber coupled calibrated attenuators in cascade. The attenuated laser pulses are then sent to the TES detection surface by a single mode optical fiber. The set of coherent states needed to perform the POVM reconstruction has been generated by lowering the initial laser pulse energy from an initial attenuation of 63.5 dB (corresponding to an average of 130 photons per pulse), to 76.5 dB (mean photon number per pulse: 6.5), to obtain 20 different states  $|\alpha_j\rangle = |\sqrt{\tau_j}\alpha\rangle$  where  $\tau_j$  is the channel transmissivity,  $j = 1, \dots, 20$ .

We work at fixed wavelength  $\lambda = 1570$  nm and thus, in ideal conditions, we would expect a discrete energy distribution with outcomes separated by a minimum energy gap  $\Delta E = \frac{hc}{\lambda}$ . Experimentally, we observe a distribution with several peaks, whose variances represent the energy resolution of the whole detection device. In a first calibration run, after a binning on the oscilloscope channels, we fit the data with a sum of independent Gaussian functions (Fig. 1 shows that the fitting functions are in excellent agreement with experimental data); the first peak on the left is the “0-peak”, corresponding to no photon detection. These fits allowed us to fix the amplitude thresholds (located close to the local minima) corresponding to  $n$  detected photons: this way, the histogram of counts is obtained just binning on the intervals identified by these thresholds. The distributions  $p_{n,j}$  are finally evaluated upon normalizing the histogram bars to the total number of events for the given state  $||$ . This threshold-based counts binning may introduce some bias or fluctuations since the tails of the  $n$ -th Gaussian peak fall out of the  $n$  counts interval. On the other hand, the effects in neighbouring peaks compensate each other and, overall, do not affect the tomographic reconstruction.

$||$  Remarkably, the reconstructions obtained by binning data using thresholds are almost indistinguishable from the ones obtained by evaluating the number of events in the  $n$ -th peak by integrating the corresponding Gaussian of the fit reported in Fig. 1.

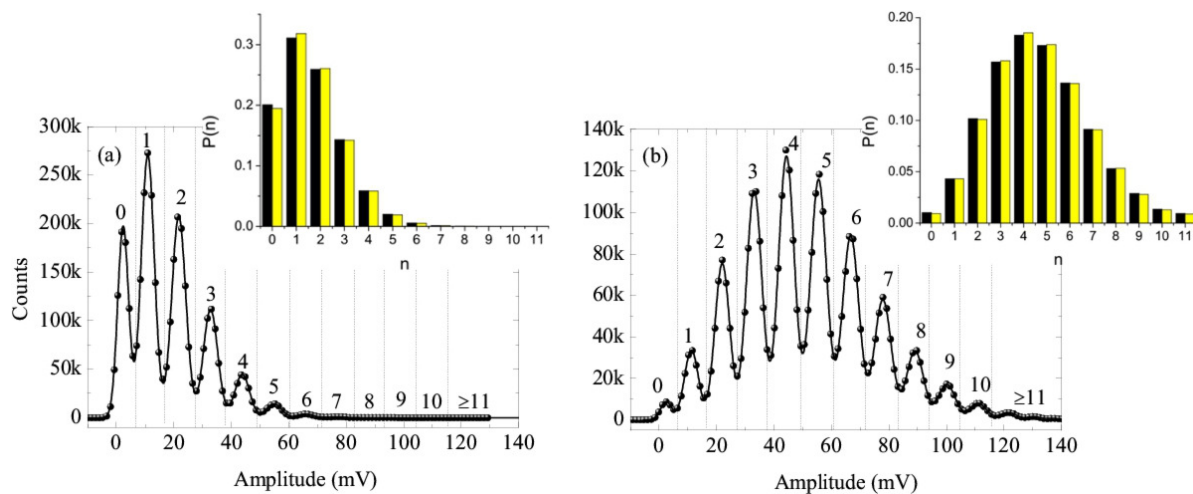


**Figure 1.** Dots represent the TES counts for two different values of  $|\alpha_j\rangle$ : each point corresponds to a binning of an amplitude interval of 1.3 mV. Solid lines are the Gaussian fits on the experimental data, while the dotted vertical lines are the thresholds. Figure (a) is obtained with a coherent state characterized by a mean photon number per pulse  $\mu = 31$ , while for figure (b) the state used had  $\mu = 87$ . The insets of both figures compare the experimental probability distribution (black bars), obtained from measurements binned according to the drawn thresholds, with the corresponding Poisson distributions of mean value  $\eta\mu$  (with  $\eta = 5.1\%$ ) (yellow bars): as evident from the plots, the experimental results are in remarkable agreement with the theoretical predictions, showing respectively a fidelity of 99.994% and 99.997%

## 4. Results

The POVM of our TES detection system has been reconstructed up to  $M = 140$  incoming photons and considering  $N = 12$  POVM elements  $\Pi_n$ ,  $n = 0, \dots, N - 1$ , with  $\Pi_{N-1} = 1 - \sum_{n=0}^{N-2} \Pi_n$  describing the probability operator for the detection of more than  $N - 2$  photons. In Fig. 2 we show the matrix elements  $\Pi_{nm}$  of the first 9 POVM operators ( $n = 0, \dots, 8$ ), for  $0 \leq m \leq 100$ . The bars represent the reconstructed  $\Pi_{nm}$ , while the solid lines denote the matrix elements of a linear detector. In fact, as mentioned above, the POVM of a linear photon counter can be expressed as a binomial distribution

$$\Pi_n = \sum_{m=n}^{\infty} B_{nm} |m\rangle \langle m| \quad (3)$$

of the the ideal photon number spectral measure with  $B_{nm} = \binom{m}{n} \eta^n (1 - \eta)^{m-n}$ , where  $\eta$  is the quantum efficiency of the detector. In order to compare the POVM elements of the linear detector, i.e.  $B_{nm}$ , with the reconstructed POVM elements  $\Pi_{nm}$  we have first to estimate the value of the quantum efficiency  $\eta$ .

This can be done on the sole basis of the experimental data using ML estimation, i.e. we average the values of  $\eta$  which maximize the log-likelihood functions

$$L_j = \sum_n N_{nj} \log \left( \sum_m B_{nm} q_{mj} \right) \quad (4)$$

where  $N_{nj}$  is the number of  $n$ -count events obtained with the  $j$ -th input state  $|\sqrt{\tau_j}\alpha\rangle$ . The overall procedure leads to an estimated value of the quantum efficiency  $\eta = (5.10 \pm 0.04)\%$ , where the uncertainty accounts for the statistical fluctuations (for each signal probe we estimated the value of  $\eta$ , and then we averaged over the ensemble).

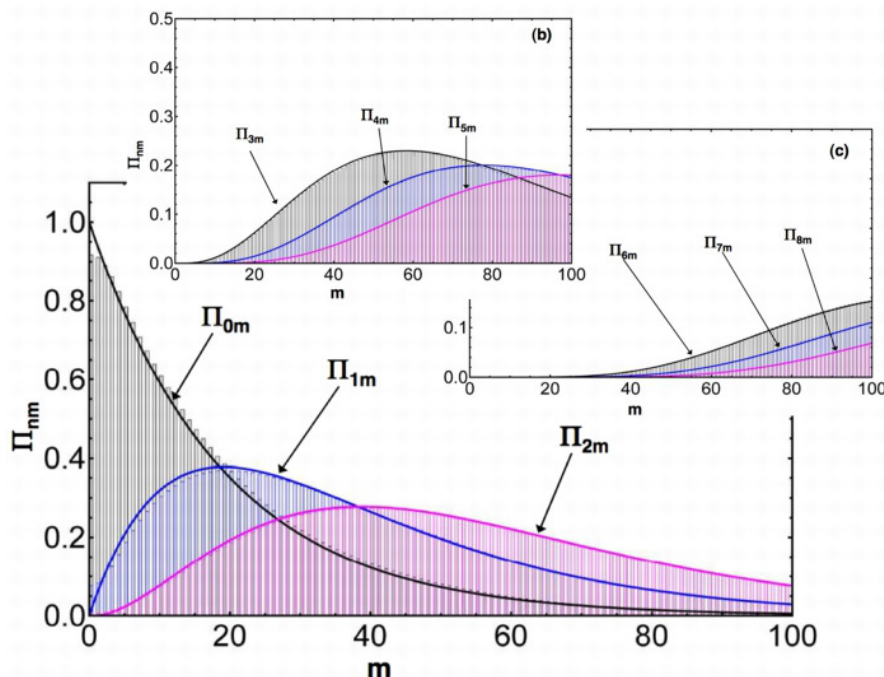


**Figure 2.** (Color Online) Reconstructed POVM of our TES photon counting systems. Bars represent the matrix elements  $\Pi_{nm}$  as a function of  $m = 0, 100$  for  $n = 0, 1, 2$  (main plot),  $n = 3, 4, 5$  (b),  $n = 6, 7, 8$  (c). Continuous lines represent the POVM elements of a linear photon counter with quantum efficiency  $\eta = 5.10\%$ .

As it is apparent from Fig. 2, we have an excellent agreement between the reconstructed POVM and the linear one with the estimated quantum efficiency. In particular, the elements of the POVM are reliably reconstructed for  $m \leq 100$ , whereas for higher values of  $m$  the quality of the reconstructions degrades. In the regime  $m \leq 100$  the fidelity  $F_m = \sum_n \sqrt{\Pi_{nm} B_{nm}}$  is larger than 0.99 (see the right inset of Fig. 3), while it degrades to 0.95 for  $100 \leq m \leq 140$ . In order to investigate the effects of experimental uncertainties, we performed a sensitivity analysis taking into account the uncertainties on the energy of the input state and on the attenuators, obtaining fidelities always greater than 98.35% for the 12 entries. In order to further confirm the linearity hypothesis, as well as to assess the reliability of the reconstruction, we have compared

the measured distributions  $p_{nj}$  with those obtained for a linear detector, i.e.

$$l_{nj} = \eta^n \exp(-\eta\mu_j) \mu_j^n / n! \quad (5)$$

and with those obtained using the reconstructed POVM elements, i.e.

$$r_{nj} = \sum_{m=n}^M \Pi_{nm} q_{mj}. \quad (6)$$

In Fig. 3 we report the three distributions for the whole set of probing coherent states, whereas in the left inset we show the (absolute) differences  $|p_{nj} - l_{nj}|$  and  $|p_{nj} - r_{nj}|$  between those distributions and the measured ones.

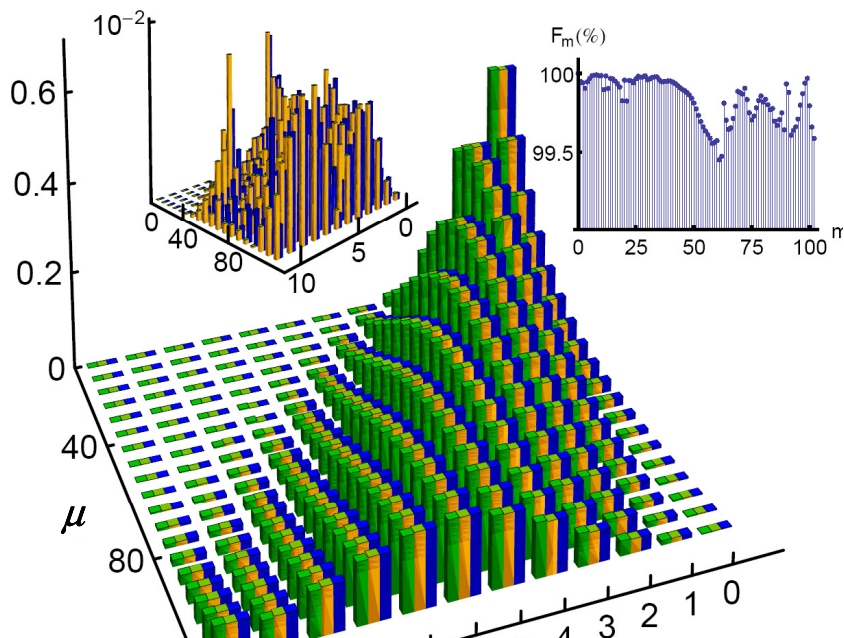


**Figure 3.** (Color Online) Comparison of the measured distributions  $p_{nj}$  (green bars, on the left of each group) of the coherent states  $|\alpha_j\rangle$  used for POVM reconstruction with those obtained using the reconstructed POVM elements  $r_{nj}$  (yellow central bars), and with those obtained under the linearity hypothesis  $l_{nj}$  (blue right bars). The left inset shows the absolute differences  $|p_{nj} - r_{nj}|$  (yellow left bars) and  $|p_{nj} - l_{nj}|$  (blue right bars). The right inset shows the fidelity  $F_m$  between the reconstructed POVM elements at fixed  $m$  and those of a linear photon counter with quantum efficiency  $\eta = 5.10\%$ .

As it is apparent from the plots, we have an excellent agreement between the different determinations of the distributions. This confirms the linear behavior of the detector, and proves that the reconstructed POVM provides a reliable description of the detection process. We have also modified the detection model to take into account the

possible presence of dark counts. In this case, upon assuming a Poissonian background, the matrix elements of the POVM are given by  $\Pi_{nm} = \exp(-\gamma) \sum_j \gamma^j / j! B_{(n-j)m}$  and we have developed a ML procedure to estimate both the quantum efficiency  $\eta$  and the mean number of dark counts per pulse  $\gamma$ . We found that the value for  $\eta$  is statistically indistinguishable from the one obtained with the linear-detector model, whereas the estimated dark counts per pulse are  $\gamma = (-0.03 \pm 0.04)$ , in excellent agreement with the direct measurement performed on our TES detector using the same fitting technique discussed above, providing a substantially negligible dark count level  $\gamma = (1.4 \pm 0.6) \times 10^{-6}$ . The same conclusion is obtained for any other model, e.g. super-Poissonian, of the background.

In conclusion, we have performed the first tomographic reconstruction of the POVM describing a TES photon detector. Our results clearly validate the description of TES detectors as linear photon counters and, together with the precise estimation of the quantum efficiency, pave the way for practical applications of TES photon counters in quantum technology.

## Acknowledgements

We acknowledge the support of the EC FP7 program ERA-NET Plus, under Grant Agreement No. 217257. MGAP thanks Stefano Olivares for useful discussions.

## References

- [1] Hadfield R H 2009 *Nat. Photonics* **3** 696
- [2] Polyakov S V and Migdall A L 2009 *J. Mod. Optic.* **56**, 1045
- [3] Zwinkels J, Ikonen E, Fox N P, Ulm G and Rastello M L 2010 *Metrologia* **47** R15
- [4] Genovese M 2005 *Phys. Rep.* **413**, 319
- [5] Brida G, Genovese M and Ruo Berchera I 2010 *Nat. Photonics* **4** 227
- [6] Langer T and Lenhart G 2009 *New J. Phys.* **11** 055051
- [7] O'Brien J L, Furusawa A and Vuckovic J 2009 *Nat. Photonics* **3** 687
- [8] Gisin N and Thew R 2007 *Nature Phot.* **1** 165
- [9] *Quantum Information, Computation and Cryptography*, Lect. Notes Phys. **808**, Benatti F, Fannes M, Floreanini R, Petritis D (Eds), (Springer, Berlin, 2010).
- [10] Jiang L A, Dauler E A and Chang J T 2007 *Phys. Rev. A* **75** 062325  
Divochiy A, Marsili F, Bitauld D, Gaggero A, Leoni R, Mattioli F, Korneev A, Seleznev V, Kaurova N, Minaeva O, Gol'tsman G, Lagoudakis K G, Benkhaoul M, Le'vy F and Fiore A 2008 *Nat. Photonics* **2** 302
- [11] Achilles D, Silberhorn Ch, Sliwa C, Banaszek K and Walmsley I A 2003 *Opt. Lett.* **28** 2387  
Fitch M J, Jacobs B C, Pittman T B and Franson J D 2003 *Phys. Rev. A* **68**, 043814
- [12] Zambra G, Bondani M, Spinelli A S and Andreoni A 2004 *Rev. Sci. Instrum.* **75** 2762
- [13] Ramilli M, Allevi A, Chmill A, Bondani M, Caccia M and Andreoni A 2010 *J. Opt. Soc. Am. B* **27** 852
- [14] Gansen E J, Rowe M A, Greene M B, Rosenberg D, Harvey T E, Su M Y, Hadfield R H, Nam S W, Mirin R P 2007 *Nat. Photonics* **1** 585
- [15] Kim J, Takeuchi S, Yamamoto Y and Hogue H H 1999 *Appl. Phys. Lett.* **74** 902  
Waks E, Inoue K, Oliver W D, Diamanti E and Yamamoto Y 2003 *IEEE J. Sel. Top. Quant.* **9** 1502

- [16] Fukuda D, Fujii G, Numata T, Amemiya K, Yoshizawa A, Tsuchida H, Fujino H, Ishii H, Itatani T, Inoue S and Zama T 2011 *Opt. Express* **19** 870
- [17] Prele D, Piat M R, Breelle E L, Voisin F, Pairat M, Atik Y, Belier B, Dumoulin L, Evesque C, Klisnick G, Marnieros S, Pajot F, Redon M and Sou G 2009 *IEEE T. Appl. Supercon.* **19** 501
- [18] Cabrera B 2008 *J. Low Temp. Phys.* **151** 82
- [19] Lita A E, Miller A J and Nam S W 2008 *Opt. Express* **16**, 3032
- [20] Rosenberg D, Lita A E, Miller A J and Nam S W 2005 *Phys. Rev. A* **71**, 061803
- [21] Bandler S R, Figueroa-Feliciano E, Iyomoto N, Kelley R L, Kilbourne C A, Murphy K D, Porter F S, Saab T and Sadleir J 2006 *Nucl. Instrum. Meth. A* **559**, 817
- [22] Irwin K D and Hilton C G, in *Cryogenic Particle Detection*, C. Enss (Ed.), Topics Appl. Phys., **99** (Springer, Berlin, 2005).
- [23] Luis A and Sanchez-Soto L L 1999 *Phys. Rev. Lett.* **83**, 3573
- [24] Fiurasek J 2001 *Phys. Rev. A* **64** 024102
- [25] Demartini F, Mazzei A, Ricci, and D'Ariano G M 2003 *Phys. Rev. A* **67**, 062307
- [26] Mitchell M W, Ellenor C W, Schneider S and Steinberg A M 2003 *Phys. Rev. Lett.* **91**, 120402
- [27] D'Ariano G M, Maccone L and Lo Presti P 2004 *Phys. Rev. Lett.* **93** 250407
- [28] Rossi A R, Olivares S and Paris M G A 2004 *Phys. Rev. A* **70**, 055801  
Zambra G, Bondani M, Andreoni A, Gramegna M, Genovese M, Brida G, Rossi A and Paris M G A 2005 *Phys. Rev. Lett.* **95**, 063602
- [29] Lobino M, Korystov D, Kupchak C, Figueroa E, Sanders B C and Lvovsky A I 2008 *Science* **322** 563
- [30] Rahimi-Keshari S, Scherer A, Mann A, Rezakhani A T, Lvovsky A I and Sanders B C, 2011 *New J. Phys.* **13**, 013006
- [31] Hradil Z, Mogilevtsev D and Rehacek J 2006 *Phys. Rev. Lett.* **96** 230401
- [32] Lundeen J S, Feito A, Coldenstrodt-Ronge H, Pregnell K L, Silberhorn Ch, Ralph T C, Eisert J, Plenio M B and Walmsley I A 2009 *Nat. Phys.* **5** 27
- [33] Rehacek J, Mogilevtsev D and Hradil Z 2010 *Phys. Rev. Lett.* **105** 010402
- [34] Baltin R 1983 *J. Phys. A-Math. Gen.* **16** 2721
- [35] Paris M G A 1996 *Phys. Rev. A* **53**, 2658
- [36] Paris M G A 1996 *Opt. Comm.* **124**, 277
- [37] Portesi C, Taralli E, Rocci R, Rajteri M and Monticone E, 2008 *J. Low Temp. Phys.* **151**, 261
- [38] Taralli E, Rajteri M, Monticone E and Portesi C 2007 *Int. J. Quantum. Inf.* **5**, 293
- [39] Drung D, Assmann C, Beyer J, Kirste A, Peters M, Ruede F and Schurig Th 2007 *IEEE T. Appl. Supercon.* **17**, 699